Dynamics of internal pore opening in K_V channels probed by a fluorescent unnatural amino acid

Tanja Kalstrup and Rikard Blunck[1]

Groupe d'étude des protéines membranaires (GÉPROM) and Departments of Physics and Physiology, Université de Montréal, Montreal, QC, Canada H3C 3J7

Edited by Francisco Bezanilla, University of Chicago, Chicago, IL, and approved April 8, 2013 (received for review November 22, 2012)

Atomic-scale models on the gating mechanism of voltage-gated potassium channels (Kv) are based on linear interpolations between static structures of their initial and final state derived from crystallography and molecular dynamics simulations, and, thus, lack dynamic structural information. The lack of information on dynamics and intermediate states makes it difficult to associate the structural with the dynamic functional data obtained with electrophysiology. Although voltage-clamp fluorometry fills this gap, it is limited to sites extracellularly accessible, when the key region for gating is located at the cytosolic side of the channels. Here, we solved this problem by performing voltage-clamp fluorometry with a fluorescent unnatural amino acid. By using an orthogonal tRNA-synthetase pair, the fluorescent unnatural amino acid was incorporated in the Shaker voltage-gated potassium channel at key regions that were previously inaccessible. Thus, we defined which parts act independently and which parts act cooperatively and found pore opening to occur in two sequential transitions.

Anap | two-color VCF

Voltage-gated potassium channels (K_V) are essential for generating action potentials in the central nervous system and, when defective, are linked to severe familial diseases including cardiac arrhythmias and epilepsy. The voltage-sensing domains (VSD) of K_V channels (transmembrane helices S1–S4; Fig. 1*A*) undergo a major conformational change upon membrane depolarization driven by the positive charges in the S4, which finally leads to opening of the pore domain (transmembrane helices S5–S6). Based on the consensus on the closed (initial) and open (final) state structures (1–6), the gating movement has been predicted; the S4 helix is projected to slide upward and tilt with respect to the membrane normal, and this movement pushes the S4–S5 linker and the S6 helix inward and closes the ion-conducting pore. However, this projection relies on linear interpolations between the closed and open state and lacks any information on dynamics or intermediate states.

As a result, the projected movement does not suffice to explain fundamental characteristics of voltage sensor and pore domain kinetics, detected as "gating" and "ionic" currents, respectively. Such functional electrophysiology measurements revealed that, first, at least one intermediate state has to exist during voltage sensor movement (7) and that, second, voltage sensor movement and pore opening do not occur simultaneously. Each channel consists of four voltage sensors controlling a single central pore. It is thought that the four voltage sensors activate independently, and only after all four have activated, the central pore opens cooperatively (8, 9). This mechanism implies that the energy generated by the movement of the first three voltage sensors has to be "conserved" in the system and has to be released to the pore during opening (10). The linear interpolations between closed and open structures leave the basis of both cooperativity and energy conservation unknown.

The most effective way to link dynamic functional and structural information of electrogenic membrane proteins is voltage-clamp fluorometry (VCF) (11, 12)—simultaneous electrophysiology and site-directed fluorescence spectroscopy monitoring local rearrangements. By labeling a specific position in the protein, rearrangements of this position can be monitored in real time and can be correlated with the functional data recorded simultaneously. VCF has been successfully used to follow movements in a variety of membrane transport proteins including ion channels (12–19), transporters (20–23), and receptors (24).

Despite its power, VCF has been restricted to rearrangements on the external surface of the transport proteins due—mainly—to the thiol-reactive chemistry used for labeling. Labeling in the cytosol has proven very difficult owing to the large number of cysteines present there. Similarly, residues buried in the protein or in the membrane were not accessible. Here, we overcame these limitations by using intrinsically fluorescent unnatural amino acids (fUAAs), which are incorporated into the protein during synthesis and, thus, do not underlie the above limitations.

Previously, unnatural amino acids with various properties have been incorporated into ion channels by injecting chemically aminoacylated tRNAs into *Xenopus* oocytes (25–27) including a fUAA (28). Here, we used a fUAA to successfully carry out VCF experiments. We achieved higher expression levels by using an orthogonal $tRNA^{Anap}_{CUA}$/tRNA-synthetase pair to introduce the fUAA 3-(6-acetylnaphthalen-2-ylamino)-2-aminopropionic acid (Anap) (29) into the protein (Fig. 1*B*). Because it is genetically encoded by an *amber* nonsense codon (TAG), no limitations are set on the site of labeling. Anap has properties similar to an organic dye, although it is only slightly more voluminous than tryptophan (Fig. 1*C*). Anap was incorporated at strategic locations in the Shaker potassium channel to follow the dynamics of their movements (*i*) on "top" of the S4, the gating segment, (*ii*) in the bottom of S1 proximal to the transition from the S4 to the S4–S5 linker and (*iii*) at the C-terminal S6 close to the cytosolic gate and the S4–S5 linker C terminus (Fig. 1*A*) (top and bottom refer to the extracellular and cytosolic surface, respectively).

Results

The gating process is initiated by the positively charged S4 moving in response to depolarization of the membrane potential. To follow the movement of the outer S4, we introduced Anap on top of S4 at position A359Anap (Fig. 1*A*). The fluorescence voltage relation (FV) featured three components, two of which coincided with the major charge movements (QV; Fig. 1 *E* and *F*), i.e., with the upward translation and tilt of the S4 moving the positive charges through the electric field. Our results not only suggested that the top of S4 rearranges during the major charge movements (11, 12, 30), but also that this rearrangement occurs in two distinct movements of S4 as evidenced by the opposite direction of the two fluorescence components (Fig. 1 *E* and *F* and Fig. S1*A*). An alternative interpretation of the fluorescence change would be that the surrounding residues changed their position; however, in other biphasic FV relations found by labeling positions proximal

Author contributions: R.B. designed research; T.K. performed research; T.K. and R.B. analyzed data; and T.K. and R.B. wrote the paper.

The authors declare no conflict of interest.

This article is a PNAS Direct Submission.

[1]To whom correspondence should be addressed. E-mail: rikard.blunck@umontreal.ca.

This article contains supporting information online at www.pnas.org/lookup/suppl/doi:10.1073/pnas.1220398110/-/DCSupplemental.

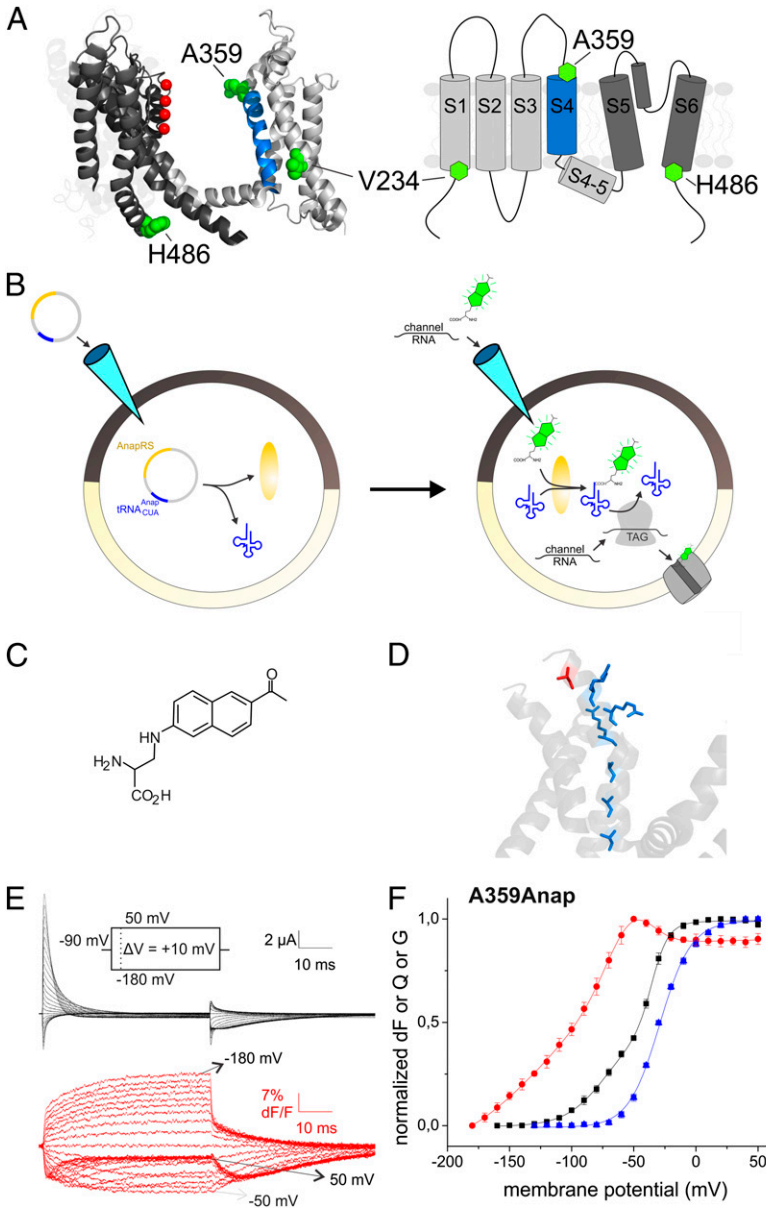

Fig. 1. (*A*) Structure of $K_V1.2/2.1$ chimera (PDB ID code 2R9R, two subunits) and topology (transmembrane segments S1–S6). The position of the mutations V234, A359, and H486 are displayed in green, and the potassium ions in the selectivity filter in red. (*B*) Principle of expression of fUAA. First, the plasmid to express the AnapRS and the corresponding tRNA is injected. On the subsequent day, fUAA and channel mRNA are injected, which leads to incorporation of the fUAA into the channel. (*C*) Structure of Anap. (*D*) Position of A359 (red) with respect to the arginines in the S4 (blue; PDB ID code 2A79). (*E*) Fluorescence response and gating currents of A359Anap in response to pulses from −90 mV to potentials between −180 and 50 mV. (*F*) Fluorescence voltage (FV, red circles), gating charge voltage (QV, black squares), and conductance voltage (GV, blue triangles) relations of A359Anap. The GV was fitted to a Boltzmann relation ($V_{1/2}$ = −29.1 mV, dV = 12.6 mV). The QV and FV were fitted to a sum of two ($V_{1/2,1}$ = −66.3 mV, dV_1 = 19.1 mV, $V_{1/2,2}$ = −35.2 mV, dV_2 = 5.4 mV) and three Boltzmann relations ($V_{1/2,1}$ = −134.6 mV, dV_1 = 32.8 mV, $V_{1/2,2}$ = −62.2mV, dV_2 =15.1 mV, $V_{1/2,3}$ = −41.6 mV, dV_3 = 11.6 mV), respectively.

to A359 atop S4 (S352 and M356) (11, 31, 32), also the two components coincided with the two major charge movements, and accessibility and VCF studies showed that the S4 itself is altering its position with respect to its surrounding during each movement (31).

Anap labeling, in contrast to organic dye labeling, enabled us to detect movements that occurred at strongly hyperpolarized potentials ($V_{1/2}$ = −134.6 mV) beyond the detectable charge movements. Cole and Moore (33) postulated, based on a delayed onset of the ionic current, a number of closed-state transitions in this voltage range occurring before the two major gating charge-carrying transitions. The fluorescence changes of A359Anap indicate that these early closed-state transitions induce structural changes in the N-terminal S4. In this voltage range, gating currents with time constants faster than 20 μs have been detected when measuring with very high bandwith (34). These gating currents might thus be related to the rearrangements we observed. Although the structural origin of these fast gating events remains unclear, charge movements in this time range have been observed to be related to an outward shift of the basic side chains in the S4 in molecular dynamics simulations (35). Such side chain "flips" were suggested earlier to occur during gating (3). This mechanism would explain why these arrangements are sensed by Anap and not by organic labels, because Anap is located right above the first arginine,

whereas an organic label, covalently linked to the –SH group of a cysteine, would be further away from the backbone (Fig. 1*D*). However, this interpretation remains highly speculative as long as in long-term simulations no separation between fast and slow events is observed (5) or until similar rearrangements are observed in simulations at lower potentials where no major charge movement occurs.

Rearrangements in the C-Terminal S4 Region. Next, we tested the dynamics of the lower S4, because no information about its movements is available yet. To this end, we introduced Anap in the lower S1 (V234Anap) in close proximity to the C terminus of the S4 helix (Fig. 1*A*). Remarkably, mutation of V234 in the N terminus of the S1 helix led to partial uncoupling of the S4 movement from pore opening, similar to different mutants in the lower S4 and S4–S5 linker (30, 36) (Fig. 2*B*). As in other uncoupled mutants, charge movement (QV) and pore opening (GV) were separated. Our finding that a mutation in the lower S1 led to uncoupling indicated that the VSD surrounding the S4 helix (S1–S3) does not merely form a passive cocoon but contributes to the gating movement. In addition, the separation between QV and GV had the advantage that it allowed us to better associate the structural rearrangements with the electrophysiological signals.

The fluorescence traces of V234Anap displayed two opposite fluorescence changes, indicating that two transitions occur in the lower S4 region (Fig. 2 *A* and *B*). The first coincided directly with the charge movement (Fig. 2*B*); the dynamics of gating charge movement superposed with the fluorescence changes of the first component (Fig. 2*C*). Considering that the upper S4 (A359Anap) also followed gating charge movement, the question arises as to whether both ends of the S4 move as one entity or whether the movement is initiated by either the upper or lower part, pulling the other one in a second transition into its final position. Comparison of the kinetics would let us gain insight into this question, however, the V234Anap mutant is partly uncoupled and, thus, kinetics intrinsically differ from the A359Anap mutant. We therefore decided to monitor the movement of both ends of the S4 in the V234Anap-W434F mutant simultaneously. To this end, we introduced the mutation A359C and chemically linked a tetramethylrhodamine (TMR) via a maleimide linker to this position. As excitation and emission spectra of Anap and TMR are well separated, we were able to obtain the kinetics of the upper S4 and of the lower S4 from the same oocyte by monitoring TMR and Anap fluorescence, respectively.

In a superposition of the fluorescence signals at voltages below pore opening, Anap fluorescence (lower S4) responded faster to a voltage change than the TMR fluorescence (upper S4; Fig. 2*C*). Fitting the traces to single exponentials revealed that the region around the lower S4 moved about twice as fast as the region around the upper S4 (Fig. 2*E*). Nevertheless, both signals followed the same voltage dependence (Fig. 2 *B* and *D*), signifying that both events are prompted by the same transition. If we had a sequential two-step process with the lower S4 region moving during the first and the upper during the second step, we would expect a temporal delay in the onset of the TMR signal, which is not observed. However, the delay would be "hidden" if the TMR also senses the first transition to a small fraction. We would still observe only one exponential. Alternatively, two fully independent transitions both triggered by the positive charges in the S4 are possible. In either case, both regions do not undergo the conformational changes simultaneously, but the upper S4 region settles slower during charge movement after the initial transition in a second, voltage-independent step. Although accessibility studies suggest that the S4 itself moves during both steps (31), we can only detect movements relative to the surrounding with fluorescence. Therefore, we are not able to clearly distinguish whether also the upper and lower

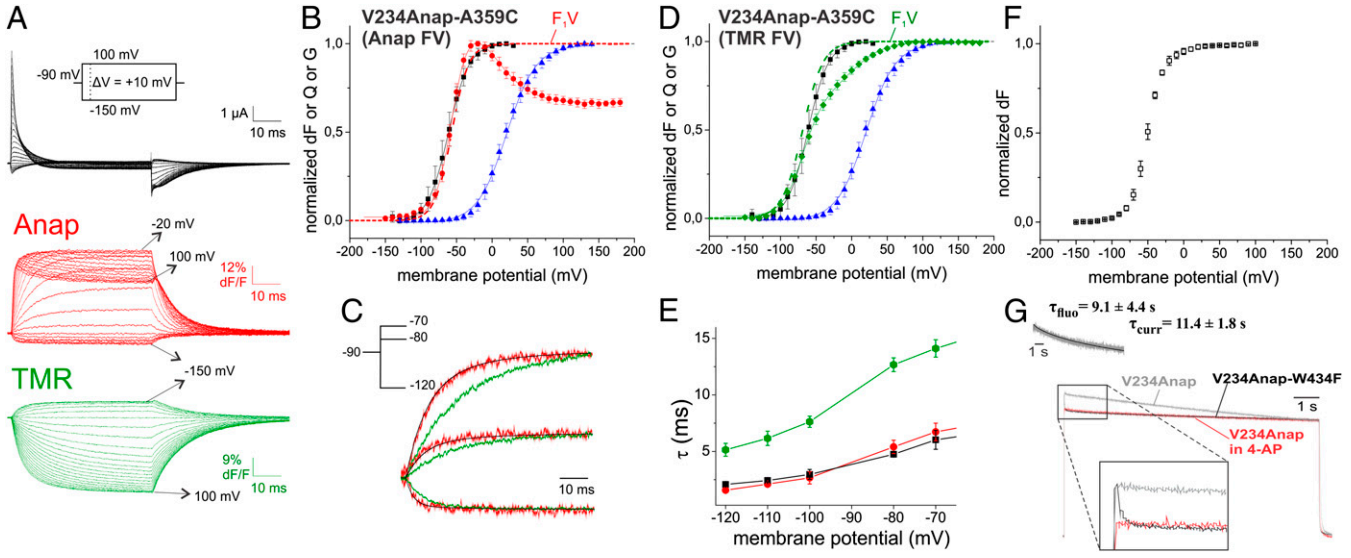

Fig. 2. (*A*) Gating currents and fluorescence responses of a TMR-labeled oocyte expressing V234Anap-A359C in response to pulses from −90 mV to potentials between −150 and 100 mV. (*B*) Anap fluorescence voltage (FV, red circles), gating charge voltage (QV, black squares) and conductance voltage (GV, blue triangles) relations of V234Anap-A359C. The GV and QV were each fitted to Boltzmann relations (GV: $V_{1/2}$ = 20.3 mV, dV = 20.6 mV; QV: $V_{1/2}$ = −61.4 mV, dV = 14.5 mV). The FV was fitted to a sum of two Boltzmann relations ($V_{1/2,1}$ = −56.7 mV, dV_1 = 11.8 mV, $V_{1/2,2}$ = −1.0 mV, dV_2 = 25.4 mV). F_1V refers to the first component of the FV. (*C*) Comparison of time dependence between charge movement (black) and fluorescence changes of V234Anap-A359C (red, Anap; green, TMR) for depolarizing pulses to voltages indicated in *Inset*. (*D*) TMR fluorescence voltage (FV, green diamonds) relation of V234Anap-A359C and the QV and GV with colors coded as in *B*. The FV was fitted to a sum of two Boltzmann relations ($V_{1/2,1}$ = −68.7 mV, dV_1 = 14.3 mV, $V_{1/2,2}$ = 0 mV, dV_2 = 23.0 mV). (*E*) Comparison among time constants of charge movement (black), Anap (red), and TMR (green) fluorescence of V234Anap-A359C. (*F*) Anap fluorescence voltage relation of the conducting mutant V234Anap. (*G*) Superposition of fluorescence traces obtained from a prolonged depolarizing pulse to 50 mV of oocytes expressing the conducting V234Anap mutant in absence (gray) or presence of 5 mM external 4-AP (red) and the nonconducting V234Anap mutant (black). The traces are normalized to the value at the end of the pulse. (*Inset*) Shown is the correlation between ionic current and fluorescence decay for the V234Anap-conducting mutant.

end of the S4 helix move differently or whether the S4 moves as one entity during one of the transitions followed by a relaxation of the surrounding around the N terminus.

C-Terminal S4 Region Moves During Opening and C-Type Inactivation. In addition to the charge-related movement, the lower S4 region undergoes another conformational change as reported by the second component in the fluorescence voltage relation. During this second transition of V234Anap-W434F, the fluorescence is decreased, whereas it increased during gating charge movement. However, in the conducting mutant V234Anap, a second component occurred with the inversed sign, i.e., the fluorescence increased and, thus, changed in the same manner as during charge movement (Fig. 2*F*). Because the amplitude of this component was small, it remained uncertain whether both signals coincided exactly. Nevertheless, the only difference between these constructs is the mutation W434F, which is thought to render the channel instantaneously C-type inactivated (37), suggesting that the lower S4 region rearranges during C-type inactivation. To confirm this hypothesis, we monitored the fluorescence signal during prolonged depolarization (Fig. 2*G*) and, indeed, fluorescence in the conducting mutant underwent a slow fluorescence decay correlating with entry to the C-type inactivated state (Fig. 2*G*). Although the W434F mutant entered the inactivated state rapidly, we were able to follow this entry because the fluorescence follows the probability of a single subunit, whereas the current is already blocked when a single of the four subunits inactivates (37) and because pore opening is likely a prerequisite. Blocking the late transitions to pore opening with the potassium channel blocker 4-aminopyridine (4-AP; refs. 38 and 39) prevented the fluorescence decrease during C-type inactivation (Fig. 2*G*).

Based on these results, we can speculate about the movement in the lower S4 region during gating. S1 and S4 likely move relative to one another during the first component, because charge movement coincides with S4 rearrangements (31) while our marker is located on the S1. The second fluorescence change occurs in the same direction, so it might be the S4 continuing in the same direction and might include the S4–S5 linker. The S4–S5 linker has been shown to move during gating (6). It is covalently linked to the S5 and also anneals to the C terminus of the S6, which forms the cytosolic gate of the ion-conducting pore (30, 40–42). Alternatively, the relative fluorescence change might be caused by a movement of the S1 or a surrounding helix. For instance, involvement of S1 and S2 in conformational changes of the voltage sensor has been demonstrated for BK (43) and Shaker channels (11). Finally, in the C-type inactivated conformation, the helices are reoriented such that fluorescence of V234Anap reduces. This movement is probably associated with the S4, because movement of the N-terminal S4 during C-type inactivation and relaxation has been shown (30, 44–47).

Final Pore Opening Occurs in a Two-Step Process. The synchronism of the voltage dependencies of the first component of the V234Anap fluorescence signal and the major charge movement signifies that lower S4 movement still occurred independently for each voltage sensor if we assume that major charge movement occurs independently for partially uncoupled mutants (32). Thus, the S4 helix does not yet contribute to the cooperative pore opening. To find the location, which no longer shows independently but only cooperatively moving components, and to answer the question how this internal pore gate behaved with respect to the lower S4, we incorporated Anap at position H486 in the C-terminal S6 close to the attachment site to the S4–S5 linker (30, 40–42, 48) (Fig. 1*A*). The corresponding FV contained two components (Fig. 3 *A* and *B* and Fig. S1*B*): The first component was situated between QV and GV, whereas the second component was closely related to the GV. Because no component superposed with the QV directly, the associated movement at the internal gate of K_V did not occur independently for the four subunits. The C-terminal S6 may thus be interpreted as the first position in the gating path not to act independently but cooperatively as postulated (8). However, this first transition did not coincide yet with the GV, indicating that, in contrast to previous models (8), the first cooperative step after activation of all four voltage sensors did not yet open the pore, but that a second transition of the internal gate is required as suggested by Schoppa and Sigworth (9) and Bezanilla et al. (7). This finding is confirmed in a superposition of the fluorescence change with the ionic current; here, movement of the C-terminal S6 evidently preceded ion conduction (Fig. 3*C*). Pore opening (GV) is finally related to the second component of the FV (Fig. 3*B*). All in all, fluorescent tracking of the internal gate revealed two features for pore opening: (*i*) Movement of the C-terminal S6 is the first cooperative movement and (*ii*) the first cooperative transition of the internal pore gate is not yet sufficient for pore opening, but a second transition is required.

Discussion

If we combine the fluorescence results in this study, we are in a position to describe the structural dynamics of the entire gating sequence from the early "pregating" closed state transitions to pore opening. The gating sequence begins at strongly hyperpolarized

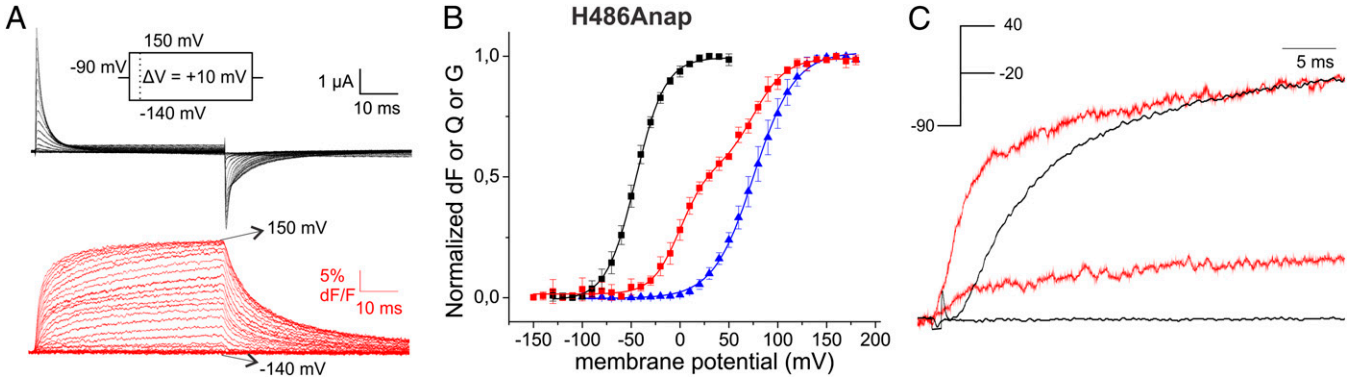

Fig. 3. (*A*) Fluorescence response and gating currents of H486Anap in response to pulses from −90 mV to potentials between −140 and 150 mV. (*B*) Fluorescence voltage (FV, red circles), gating charge voltage (QV, black squares), and conductance voltage (GV, blue triangles) relations of H486Anap. QV and GV were fitted to Boltzmann relations (QV: $V_{1/2}$ = −47.2 mV, dV = 16.2 mV; GV: $V_{1/2}$ = 75.7mV, dV = 20.9 mV). The FV was fitted to a sum of two Boltzmann relations ($V_{1/2,1}$ = 0.5 mV, dV_1 = 14.2 mV, $V_{1/2,2}$ = 75.7 mV, dV_2 = 16.4 mV. (*C*) Comparison of time dependence between conductance (black) and fluorescence (red) of H486Anap. Fluorescence changes are observed in the absence of ion conduction and clearly precede ion conduction at −20 mV and +40 mV, respectively.

potentials with closed-state transitions only observed at the N-terminal S4. It is followed by the predicted translocation and tilt of the S4 generating the two major gating charges. Despite identical voltage dependence of both the C- and N-terminal ends of S4 during the major charge movement, the conformational changes in both regions are not simultaneous. Instead, the upper S4 region "slowly" eases into its final state. The movement observed around the C-terminal S4 still occurs independently for every voltage sensor. The first cooperative movement in the gating sequence, once all voltage sensors have activated, is the first transition of the C-terminal S6, during which the pore enters an additional permissive, nonconducting state. It is followed by the final pore opening step (second S6 transition). Finally, the voltage sensor undergoes a global rearrangement during C-type inactivation and the related relaxation.

We can also compare the structural information obtained by the fluorescence measurements with the kinetic models based on electrophysiology. Although initially a single concerted step during pore opening was proposed by kinetic modeling (8), two concerted steps had been predicted in some models (7, 9). Schoppa and Sigworth (9) suggested three independent steps of each voltage sensor followed by two concerted transitions. In good agreement, we also found three transitions in the voltage sensor—one during the deep-closed states and two during major gating charge movement—followed by two concerted steps, which we detected at the C-terminal S6 in the pore domain.

Mannuzzu and Isacoff (32) found the second major charge movement in the S4 (Q_2) to show cooperativity, and they suggested this cooperativity either to be an intrinsic property of the voltage sensors or to be imposed by a cooperative subsequent transition. If the energetic coupling between pore domain and voltage sensor is strong, the cooperativity would be detected in the voltage sensor transitions although they are intrinsically independent. Energetic uncoupling of both domains in the L382V mutant removed the cooperativity in Q_2 confirming the intrinsically independent movement of the voltage sensors (32). The partial uncoupling in V234Anap and H486Anap allowed us, too, to separate the late transitions leading to pore opening, and our data seem to confirm that the concerted movements begin in the pore domain.

This effect of partial uncoupling leads to the question of energetic coupling between voltage sensor and pore domain. Remarkably, the final pore opening step that we detected was not related to major charge movement in the voltage sensor but seemed to have its own voltage dependence. Such a final voltage-dependent step for pore opening was postulated in models explaining the coupling between voltage sensing and pore domains—the electromechanical coupling (10, 30, 48–50). The separation between charge movement and pore opening by uncoupling demonstrates that energy is transferred between voltage sensors and pore domain during gating. Because the first three voltage sensors move before pore opening, the generated energy has to be conserved in the system. It is transferred to the pore domain during gating most likely via the structure separating the independent from the concerted movements. According to our results, this structure would be the S4–S5 linker annealed to the C-terminal S6. This finding is in accordance with earlier ones that mutations in the S4–S5 linker, and the C-terminal S6 lead to energetic uncoupling of voltage sensing and pore domain (30, 40, 49–51).

Our use of a fUAA provided dynamic structural information collected from the cytosolic side of the channel. VCF from the cytosolic side of the channel was not possible with chemical labeling because of the large number of unwanted binding sites in the cytosol. Labeling with fUAAs also disposes of the need to construct cysteine-free mutants, which are often impaired in function and expression. Anap has a size comparable to tryptophan and may be introduced at virtually any position in the protein. The smaller size compared with organic dyes makes it more sensitive even to small rearrangements (as seen in A359Anap). Because fUAAs may be readily incorporated in any protein with minimal genetic manipulation, we expect voltage-clamp fluorometry in combination with fUAAs to find widespread application in structural biology.

Materials and Methods

Molecular Biology and Channel Expression. Mutations were introduced into a plasmid encoding the *Drosophila* Shaker gene H4 in the pBSTA vector with N-type inactivation removed by deletion of amino acids 6–46 (52). Gating currents and fluorescence traces were obtained from the nonconducting W434F mutant. The tRNA/AnapRS encoding plasmid and the fUAA Anap (29) were kindly provided by Peter G. Schultz (Scripps Research Institute, La Jolla, CA). For functional expression of channels harboring Anap, 0.5 ng of cDNA encoding the tRNA/AnapRS pair was injected into the nucleus of oocytes from *Xenopus laevis* situated in the animal pole and incubated for 24 h at 18 °C to allow tRNA transcription and synthetase expression. Subsequent steps were performed under light not exciting the fluorophore (>610 nm). 5–35 nanograms of in vitro transcribed RNA was coinjected with 23 nL of 1 mM Anap. Oocytes were incubated in Barth solution for 1–3 d at 18 °C. In the absence of the tRNA/AnapRS pair and/or the fUAA, no channel expression was detected for all three mutants, verifying that only proteins with the inserted unnatural amino acids were trafficked to the membrane.

Voltage-Clamp Fluorometry. Voltage clamp was performed with a CA-1B amplifier (Dagan). Currents were recorded in the cut-open oocyte voltage-clamp configuration as described (30) and analyzed by using GPatch (Department of Anesthesiology, University of California, Los Angeles). Capacitive currents were subtracted from gating currents by using the P/4 protocol (53). For fluorescence measurements, an upright fluorescence microscope (Axioskop 2FS; Zeiss) and a Photomax 200 photodetection system (Dagan) were used. Boltzmann relations were of the form $y = (1+\exp((V_{1/2}-V)/dV))^{-1}$ and $y = (1+\exp((V_{1/2,1}-V)/dV_1)(1+\exp((V_{1/2,2}-V)/dV_2))^{-1}$ for first (single transition) and second (for two sequential transitions) order, respectively. Data are shown as mean ± SD with n = 4–7 of at least two independent injections.

The external solution used for ionic current recordings contained 5 mM KOH, 110 mM NMDG, 10 mM Hepes, and 2 mM $Ca(OH)_2$, whereas for gating conditions, 115 mM NMDG, 10 mM Hepes, and 2 mM $Ca(OH)_2$ was used. The internal solution contained 115 mM NMDG (gating) or KOH (ionic), 10 mM Hepes, and 2 mM EDTA. TMR labeling was accomplished by incubating oocytes for 20 min in 5 μM TMR-maleimide (Invitrogen) in depolarizing solution [115 mM KOH, 10 mM Hepes, and 2 mM $Ca(OH)_2$]. All solutions were adjusted to pH 7.1 with Mes.

ACKNOWLEDGMENTS. The plasmid encoding the tRNA/AnapRS pair and Anap were kind gifts from Dr. Peter G. Schultz (Scripps Research Institute, La Jolla, CA). We thank Dr. Abhishek Chatterjee for advice on plasmid preparation, Helène Klein for discussions on unnatural amino acid expression, and Yolaine Dodier and Yoan Lussier for technical assistance. This work was funded by the Canadian Institutes for Health Research Grant MOP-102689 (to R.B.) and Canadian Foundation for Innovation Grant 950-225005. Groupe d'Études des Protéines Membranaires is a research group funded by the Fonds de recherche du Québec–Santé. R.B. holds a Canada Research Chair on Molecular Mechanisms of Membrane Proteins.

1. Long SB, Tao X, Campbell EB, MacKinnon R (2007) Atomic structure of a voltage-dependent K+ channel in a lipid membrane-like environment. *Nature* 450(7168): 376–382.
2. Long SB, Campbell EB, Mackinnon R (2005) Crystal structure of a mammalian voltage-dependent Shaker family K+ channel. *Science* 309(5736):897–903.
3. Yarov-Yarovoy V, et al. (2012) Structural basis for gating charge movement in the voltage sensor of a sodium channel. *Proc Natl Acad Sci USA* 109(2):E93–E102.
4. Vargas E, Bezanilla F, Roux B (2011) In search of a consensus model of the resting state of a voltage-sensing domain. *Neuron* 72(5):713–720.
5. Jensen MO, et al. (2012) Mechanism of voltage gating in potassium channels. *Science* 336(6078):229–233.
6. Faure E, Starek G, McGuire H, Bernèche S, Blunck R (2012) A limited 4 Å radial displacement of the S4-S5 linker is sufficient for internal gate closing in Kv channels. *J Biol Chem* 287(47):40091–40098.
7. Bezanilla F, Perozo E, Stefani E (1994) Gating of Shaker K+ channels: II. The components of gating currents and a model of channel activation. *Biophys J* 66(4):1011–1021.
8. Zagotta WN, Hoshi T, Aldrich RW (1994) Shaker potassium channel gating. III: Evaluation of kinetic models for activation. *J Gen Physiol* 103(2):321–362.

9. Schoppa NE, Sigworth FJ (1998) Activation of Shaker potassium channels. III. An activation gating model for wild-type and V2 mutant channels. *J Gen Physiol* 111(2):313–342.
10. Blunck R, Batulan Z (2012) Mechanism of electromechanical coupling in voltage-gated potassium channels. *Front Pharmacol* 3:166.
11. Cha A, Bezanilla F (1997) Characterizing voltage-dependent conformational changes in the Shaker K+ channel with fluorescence. *Neuron* 19(5):1127–1140.
12. Mannuzzu LM, Moronne MM, Isacoff EY (1996) Direct physical measure of conformational rearrangement underlying potassium channel gating. *Science* 271(5246): 213–216.
13. Cha A, Bezanilla F (1998) Structural implications of fluorescence quenching in the Shaker K+ channel. *J Gen Physiol* 112(4):391–408.
14. Bannister JP, Chanda B, Bezanilla F, Papazian DM (2005) Optical detection of rate-determining ion-modulated conformational changes of the ether-à-go-go K+ channel voltage sensor. *Proc Natl Acad Sci USA* 102(51):18718–18723.
15. Savalli N, Kondratiev A, Toro L, Olcese R (2006) Voltage-dependent conformational changes in human Ca(2+)- and voltage-activated K(+) channel, revealed by voltage-clamp fluorometry. *Proc Natl Acad Sci USA* 103(33):12619–12624.
16. Claydon TW, Fedida D (2007) Voltage clamp fluorimetry studies of mammalian voltage-gated K(+) channel gating. *Biochem Soc Trans* 35(Pt 5):1080–1082.
17. Blunck R, Starace DM, Correa AM, Bezanilla F (2004) Detecting rearrangements of shaker and NaChBac in real-time with fluorescence spectroscopy in patch-clamped mammalian cells. *Biophys J* 86(6):3966–3980.
18. Zheng J, Zagotta WN (2000) Gating rearrangements in cyclic nucleotide-gated channels revealed by patch-clamp fluorometry. *Neuron* 28(2):369–374.
19. Cha A, Ruben PC, George AL, Jr., Fujimoto E, Bezanilla F (1999) Voltage sensors in domains III and IV, but not I and II, are immobilized by Na+ channel fast inactivation. *Neuron* 22(1):73–87.
20. Meinild AK, Hirayama BA, Wright EM, Loo DD (2002) Fluorescence studies of ligand-induced conformational changes of the Na(+)/glucose cotransporter. *Biochemistry* 41(4):1250–1258.
21. Gagnon DG, et al. (2005) Membrane topology of loop 13-14 of the Na+/glucose cotransporter (SGLT1): A SCAM and fluorescent labelling study. *Biochim Biophys Acta* 1712(2):173–184.
22. Li M, Farley RA, Lester HA (2000) An intermediate state of the gamma-aminobutyric acid transporter GAT1 revealed by simultaneous voltage clamp and fluorescence. *J Gen Physiol* 115(4):491–508.
23. Li M, Lester HA (2002) Early fluorescence signals detect transitions at mammalian serotonin transporters. *Biophys J* 83(1):206–218.
24. Dahan DS, et al. (2004) A fluorophore attached to nicotinic acetylcholine receptor beta M2 detects productive binding of agonist to the alpha delta site. *Proc Natl Acad Sci USA* 101(27):10195–10200.
25. Nowak MW, et al. (1995) Nicotinic receptor binding site probed with unnatural amino acid incorporation in intact cells. *Science* 268(5209):439–442.
26. Tao X, Lee A, Limapichat W, Dougherty DA, MacKinnon R (2010) A gating charge transfer center in voltage sensors. *Science* 328(5974):67–73.
27. Pless SA, Galpin JD, Niciforovic AP, Ahern CA (2011) Contributions of counter-charge in a potassium channel voltage-sensor domain. *Nat Chem Biol* 7(9):617–623.
28. Pantoja R, Rodriguez EA, Dibas MI, Dougherty DA, Lester HA (2009) Single-molecule imaging of a fluorescent unnatural amino acid incorporated into nicotinic receptors. *Biophys J* 96(1):226–237.
29. Lee HS, Guo J, Lemke EA, Dimla RD, Schultz PG (2009) Genetic incorporation of a small, environmentally sensitive, fluorescent probe into proteins in Saccharomyces cerevisiae. *J Am Chem Soc* 131(36):12921–12923.
30. Haddad GA, Blunck R (2011) Mode shift of the voltage sensors in Shaker K+ channels is caused by energetic coupling to the pore domain. *J Gen Physiol* 137(5):455–472.
31. Baker OS, Larsson HP, Mannuzzu LM, Isacoff EY (1998) Three transmembrane conformations and sequence-dependent displacement of the S4 domain in shaker K+ channel gating. *Neuron* 20(6):1283–1294.
32. Mannuzzu LM, Isacoff EY (2000) Independence and cooperativity in rearrangements of a potassium channel voltage sensor revealed by single subunit fluorescence. *J Gen Physiol* 115(3):257–268.
33. Cole KS, Moore JW (1960) Potassium ion current in the squid giant axon: Dynamic characteristic. *Biophys J* 1:1–14.
34. Sigg D, Bezanilla F, Stefani E (2003) Fast gating in the Shaker K+ channel and the energy landscape of activation. *Proc Natl Acad Sci USA* 100(13):7611–7615.
35. Freites JA, Schow EV, White SH, Tobias DJ (2012) Microscopic origin of gating current fluctuations in a potassium channel voltage sensor. *Biophys J* 102(11):L44–L46.
36. Ledwell JL, Aldrich RW (1999) Mutations in the S4 region isolate the final voltage-dependent cooperative step in potassium channel activation. *J Gen Physiol* 113(3): 389–414.
37. Yang Y, Yan Y, Sigworth FJ (1997) How does the W434F mutation block current in Shaker potassium channels? *J Gen Physiol* 109(6):779–789.
38. McCormack K, Joiner WJ, Heinemann SH (1994) A characterization of the activating structural rearrangements in voltage-dependent Shaker K+ channels. *Neuron* 12(2): 301–315.
39. Loboda A, Armstrong CM (2001) Resolving the gating charge movement associated with late transitions in K channel activation. *Biophys J* 81(2):905–916.
40. Lu Z, Klem AM, Ramu Y (2001) Ion conduction pore is conserved among potassium channels. *Nature* 413(6858):809–813.
41. Labro AJ, et al. (2008) Kv channel gating requires a compatible S4-S5 linker and bottom part of S6, constrained by non-interacting residues. *J Gen Physiol* 132(6): 667–680.
42. Long SB, Campbell EB, Mackinnon R (2005) Voltage sensor of Kv1.2: Structural basis of electromechanical coupling. *Science* 309(5736):903–908.
43. Pantazis A, Olcese R (2012) Relative transmembrane segment rearrangements during BK channel activation resolved by structurally assigned fluorophore-quencher pairing. *J Gen Physiol* 140(2):207–218.
44. Pathak M, Kurtz L, Tombola F, Isacoff E (2005) The cooperative voltage sensor motion that gates a potassium channel. *J Gen Physiol* 125(1):57–69.
45. Gandhi CS, Loots E, Isacoff EY (2000) Reconstructing voltage sensor-pore interaction from a fluorescence scan of a voltage-gated K+ channel. *Neuron* 27(3):585–595.
46. Claydon TW, Vaid M, Rezazadeh S, Kehl SJ, Fedida D (2007) 4-aminopyridine prevents the conformational changes associated with p/c-type inactivation in shaker channels. *J Pharmacol Exp Ther* 320(1):162–172.
47. Villalba-Galea CA, Sandtner W, Starace DM, Bezanilla F (2008) S4-based voltage sensors have three major conformations. *Proc Natl Acad Sci USA* 105(46): 17600–17607.
48. Batulan Z, Haddad GA, Blunck R (2010) An intersubunit interaction between S4-S5 linker and S6 is responsible for the slow off-gating component in Shaker K+ channels. *J Biol Chem* 285(18):14005–14019.
49. Muroi Y, Arcisio-Miranda M, Chowdhury S, Chanda B (2010) Molecular determinants of coupling between the domain III voltage sensor and pore of a sodium channel. *Nat Struct Mol Biol* 17(2):230–237.
50. Ding S, Horn R (2003) Effect of S6 tail mutations on charge movement in Shaker potassium channels. *Biophys J* 84(1):295–305.
51. Schoppa NE, Sigworth FJ (1998) Activation of Shaker potassium channels. II. Kinetics of the V2 mutant channel. *J Gen Physiol* 111(2):295–311.
52. Hoshi T, Zagotta WN, Aldrich RW (1990) Biophysical and molecular mechanisms of Shaker potassium channel inactivation. *Science* 250(4980):533–538.
53. Bezanilla F, Armstrong CM (1977) Inactivation of the sodium channel. I. Sodium current experiments. *J Gen Physiol* 70(5):549–566.